Creep Behavior of Al-Si Die-Cast Alloys

Tim Jaglinski

Roderic Lakes

Materials Science Program and Engineering Physics Department,
University of Wisconsin-Madison

Commercial, aluminum die-cast alloys are subject to long-term stresses leading to viscoelastic material responses resulting in inefficient engine operation and failure. Constant load creep tests were conducted on aluminum die-casting alloys: B-390, eutectic Al-Si and a 17% Si-Al alloys. Rupture occurred in the primary creep regime, with the eutectic alloy having the longest times to failure. Primary creep was modeled by $J(t)=A+Bt^n$ with A, B, and n dependent on stress. Poor creep performance is linked to the brittle fracture of the primary silicon phase as well as other casting defects. [DOI: 10.1115/1.1789953]

1 Introduction

Currently, small engine design is done with the designer's awareness of the viscoelastic nature of their materials. We consider viscoelasticity to include time dependent behavior which may be nonlinear or partially non-recoverable. Non-recoverable time-dependent behavior may also be described as viscoplastic. Work has been done on creep in pure aluminum [1,2], various aluminum alloys [3,4] and aluminum composites with SiC particulates [5,6], however experimental data for die-cast aluminum alloys is sparse. In addition, because die-casting is an extremely variable process from manufacturer to manufacturer (in regards to gating methods, mold sizes, pressures and temperatures) and in conjunction with the fact that die-cast alloys have been traditionally known to exhibit poor creep resistance, the study of die-cast aluminum alloys has been largely neglected by academia in favor of alloys that are theoretically more creep resistant, such as the nickel based superalloys [7].

Despite the lack of high-temperature data, the die-casting process is still widely used due to the ability to achieve high part volumes and tight part tolerances at low-cost [8]. More than ever, the market is demanding more efficient engines that run with little or no post-factory maintenance over the operating life of the engine. These increased performance demands are forcing designers to take creep and relaxation phenomena into account to meet their design goals, thus creating the need to determine the high-temperature properties of their specific commercial alloys. In addition, since this industry provides a high volume and inexpensive product, the ability to employ techniques such as directional solidification or the use of advanced alloys to minimize viscoelastic responses are not feasible due to the very high cost of these manufacturing methods.

The most important viscoelastic phenomena occurring in engine components are creep and relaxation. Creep is a material's strain response to a constant stress over time, whereas relaxation is the stress response due to a constant strain over time [9]. In both cases these processes can lead to degraded engine performance. Component failure or loss of tolerance is attributed to creep; and relaxation, occurring largely in bolted joints, can contribute to engine deficiency through seal leakage and piston blow-by.

Creep of most materials can be separated into three phases; primary creep where the strain rate decreases with time, secondary creep with a constant strain rate and lastly, tertiary creep where the strain rate accelerates to fracture [7,9]. Extensive analysis can be found in the literature for materials exhibiting a steady-state creep rate [10]. Secondary creep is normally described using some form of the Dorn equation typically given by [10]

$$\dot{\varepsilon}_{ss}=A\left(\frac{b}{d}\right)^p\left(\frac{D_oGb}{kT}\right)\left(\frac{\sigma}{G}\right)^n\exp\left(\frac{-Q_c}{RT}\right) \tag{1}$$

where b is the Burgers Vector, d is the grain size, D_o is the self diffusion coefficient, G is the shear modulus, σ is the applied stress, k is Boltzmann's constant, Q_c is the activation energy for creep, R is the universal gas constant, T is the absolute temperature and A, p, and n are dimensionless constants. This equation has been used as a phenomenological curve fit where integer values of the constant n (usually 1–8) can be correlated to various creep mechanisms including multiple forms of dislocation motion and grain boundary sliding [4,11,12].

Equation (1) is only useful if the material exhibits a steady-state creep rate. Furthermore, in most engineering applications the allowable strains are small. Consequently, it is expected that components in service never reach the secondary phase, or worse, the tertiary stage, for safety and performance requirements. Modeling of the primary phase would be far more useful, but is difficult [7]. In addition, Eq. (1) provides no information on the time to failure by fracture or ''failure'' by the attainment of some allowable threshold strain. This is extremely important for design as the material can fracture in any of the creep regimes.

A suggested curve-fit for the high temperature primary creep region is given by [7,13]

$$\varepsilon_p=\varepsilon_o+A(\sigma,T)t^n \tag{2}$$

where ε_p is the primary creep strain, ε_o is the elastic strain, t is time, n is the rate exponent, not to be confused with the creep exponent in Eq. (1), and A is a time-independent constant that can depend on stress and temperature. It has been shown that for a large variety of materials n has a value on the order of 1/3, commonly referred to as Andrade's Law [13,14]. For more flexibility, a series of power laws can also be used [9].

$$\varepsilon_p=\sum_{m=1}^{n}A_m(\sigma,T)t^{n(\sigma,T)_m} \tag{3}$$

Again, Eqs. (2) and (3) are only curve-fits which can be used for design if the stress and temperature dependence of A and n can be determined. This can be done by doing a range of creep tests over the material's entire stress and temperature operating envelope.

The activation energy for creep can be determined if the obtained empirical creep curves for one stress and various temperatures can be superimposed on each other to form a master curve. This can be done by time-temperature superposition through application of the Arrhenius rate equation [15].

$$t=t_o\exp\left(\frac{Q_c}{RT}\right) \tag{4}$$

and

Contributed by the Materials Division for publication in the JOURNAL OF ENGINEERING MATERIALS AND TECHNOLOGY. Manuscript received by the Materials Division May 13, 2003; revised manuscript received May 17, 2004. Associate Editor: A. M. Rajendran.

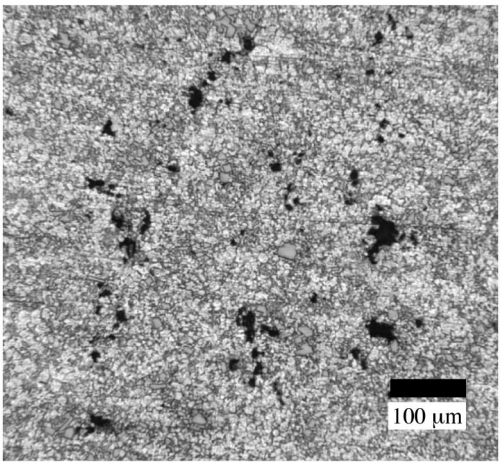

(*a*)

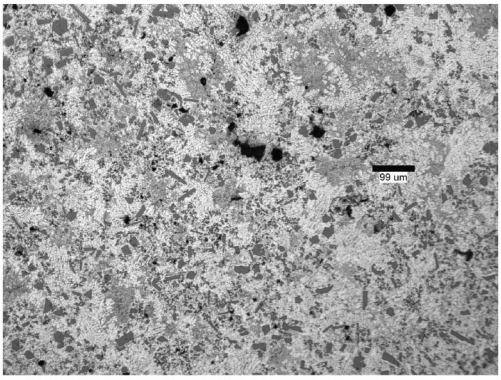

(*b*)

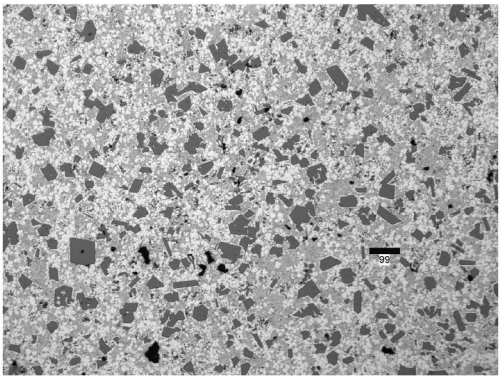

(*c*)

Fig. 1 (*a*) As-cast microstructure of the eutectic Al-Si alloy; (*b*) as-cast microstructure of the B390 commercial alloy; and (*c*) as-cast microstructure of the Al-17Si alloy.

$$\ln\left(\frac{t_1}{t_2}\right)=\frac{Q_c}{R}\left(\frac{1}{T_1}-\frac{1}{T_2}\right) \tag{5}$$

where t_o is some characteristic time. By taking empirical data and determining the time ratio required to superimpose two creep curves at different temperatures and the same stress, the activation energy for creep, Q_c, can be determined [9,15]. The process can be repeated for other stress levels to determine the stress dependence of Q_c

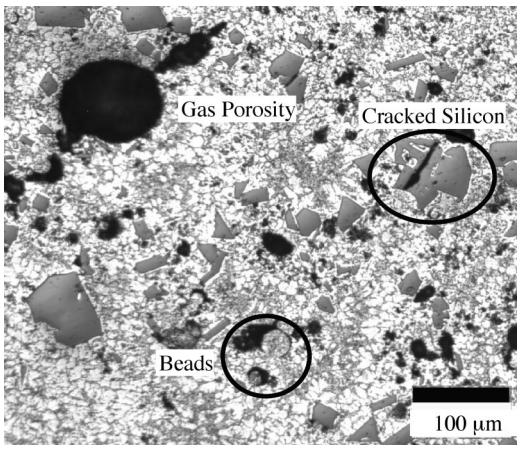

Fig. 2 Micrograph of a fractured Al-17Si creep specimen near the fracture surface demonstrating the presence of gas porosity and aluminum beads and their possible influence on crack growth

2 Experimental Methods and Materials

All test bars were supplied by commercial die-cast component manufacturers. As-cast tensile specimens were used with gauge dimensions of $2.5''\times0.25''$ diameter and $2.5''\times0.245''$ diameter due to two different specimen sources. The alloy compositions were as follows: B390 as Al-17Si-4Cu-0.5Mg, Eutectic Al-13Si-3Cu-0.2Mg (hereafter referred to as eutectic), and Al-17Si-0.2Cu-0.5Mg-1.2Fe (referred to hereafter as Al-17Si) in weight percent.

Constant load creep uniaxial tests were conducted using a dead-weight lever frame. Strain was measured using a full bridge of discrete strain gauges, with two gauges located on a temperature compensation (dummy) sample comprised of the same test material. WK 350 Ohm gauges were used on all samples and dummies. The initial 200 sec of each test was captured using a digital oscilloscope. Data after 200 sec were taken manually using a digital voltmeter in such a way as to approximate logarithmic time steps. The first data point is not reported until after the first 10 sec of each test since the rise-time of the load history was about 1 sec. Preload on the sample from the fixturing was on the order of 20 $\mu\varepsilon$. Once in the testing fixture, the sample was brought to temperature and allowed to maintain steady state for at least twelve hours prior to application of load.

Samples for optical micrographs were prepared from crept specimens using a low-speed diamond saw. The specimens were potted and pucks were wet-ground using silica sandpapers, with coarse polishing done using a 1.0 micron diamond paste and fine polishing using a 0.03–0.06 micron colloidal silica solution. After polishing, samples were etched with a 0.5 percent HF solution. Micrographs were taken using an optical microscope equipped with a digital camera and accompanying software on a PC.

Tests for blistering were done by bringing an oven to a temperature of 480° C and placing the as received samples inside for 1 hour. The density measurements where made using the protocol provided with a ME-33360 Mettler Balance density determination kit. This method compares the sample's effective mass when dry and when immersed in water, using Eq. (6).

$$\rho=\frac{\rho_w m_d}{(m_d-m_s)} \tag{6}$$

Here ρ_w is the density of water, m_d is the dry mass of the sample and m_s is the suspended mass when immersed in the reference liquid.

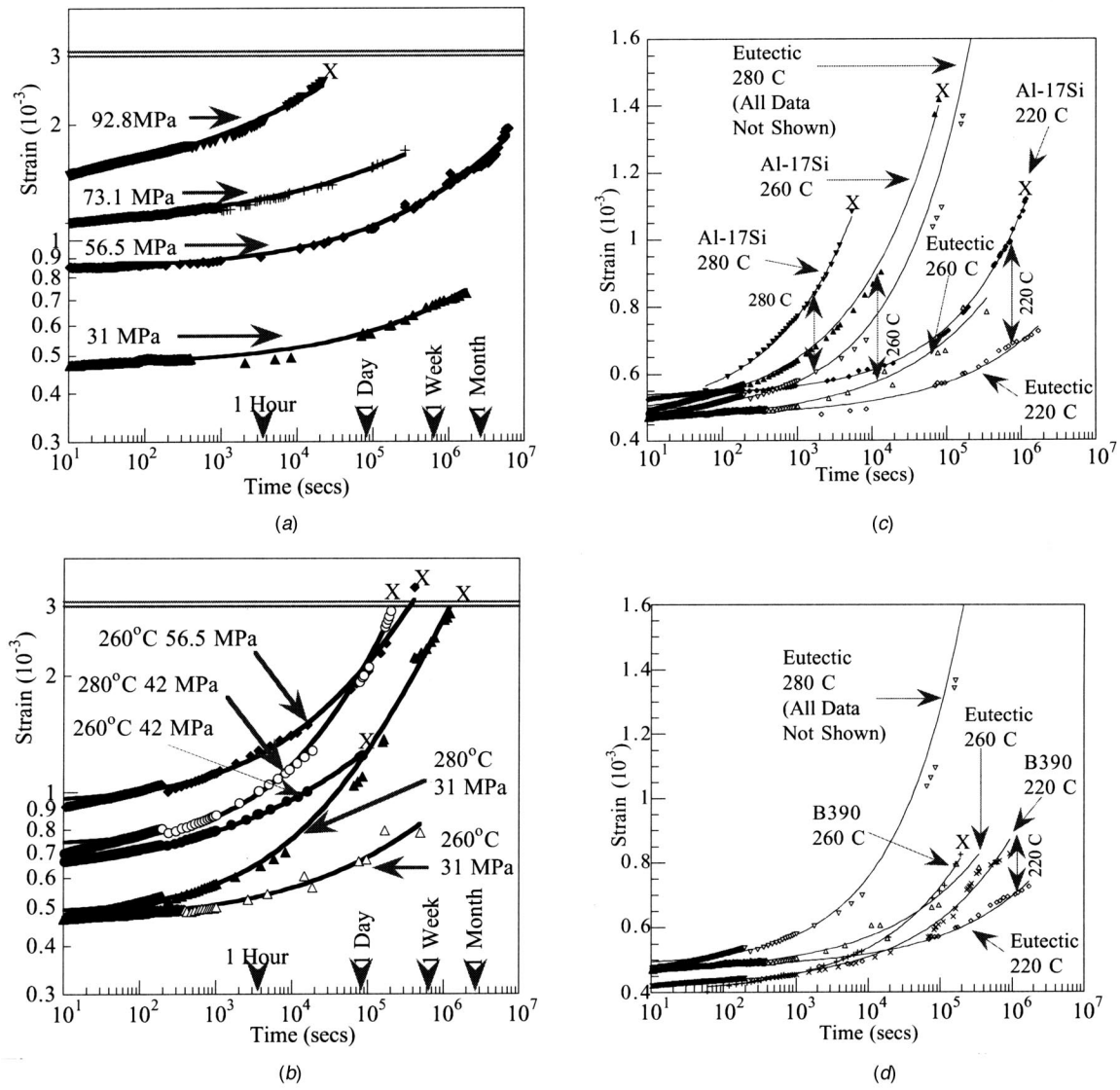

Fig. 3 (*a*) **Creep results obtained for the eutectic Al-Si alloy for 220°C. Curves with *X*'s are to fracture, those without were stopped due to time constraints. Curve-fits are of the form shown in Eq. (2);** (*b*) **creep results obtained for the eutectic Al-Si alloy for 260° and 280°C. Curves with *X*'s are to fracture, those without were stopped due to time constraints. Curve-fits are of the form shown in Eq. (2);** (*c*) **comparison of creep results between the eutectic and Al-17Si alloys at the same stress of 32MPa and various temperatures, *X* indicates specimen rupture; and** (*d*) **comparison of creep results between the eutectic and B390 Al-Si alloys at the same stress of 32MPa and various temperatures.**

3 Results and Discussion

Figures 1(*a*–*c*) are typical field photo-micrographs of the as-cast microstructures in the gauge sections of the eutectic, B390 and the Al-17Si alloys respectively. Qualitatively, the Al-17Si has the highest aggregation of the primary silicon phase with the largest particle sizes on the order of 50 μm, the B390 is less aggregated with the largest particles sizes on the order of 20 μm. The eutectic has the most refined microstructure with silicon particle sizes of 5 μm or less, although isolated particles can be found up to 10 μm in size. The presence of some intermetallic particles can also be found in the eutectic alloy.

Besides the differing microstructures, each alloy had varying degrees of entrapped gas porosity and aluminum beads, which are typical defects from the die-casting process. Figure 2 shows a micrograph of a failed specimen of the Al-17Si alloy near the fracture surface where both gas porosity and aluminum beads are visible. Both defects act, at a minimum, to decrease the load bearing cross section and as crack nucleation sites. The size and quantity of both defects will decrease the rupture time as grain boundary cavities do not have to nucleate from collections of vacancies [4,16] as well as randomizing time to failure. Moreover, the gas porosities will exert a compressive radial stress, σ_r, and a tensile circumferential stress, σ_θ, on the surrounding matrix. During the die-casting process trapped bubbles are highly compressed volumetrically and then frozen during solidification. Upon reheating these bubbles tend to expand, which can give rise to blistering. It was found that samples simply exposed to a temperature of 480°C for 1 hour showed significant localized swelling, or a decrease in local density. For example, one measured cylindrical gauge section underwent a decrease in density from 2.7 to 2.4 g/cm^3. It should be noted that this result is only a worst case example and is intended only to demonstrate that the effects of entrapped gas

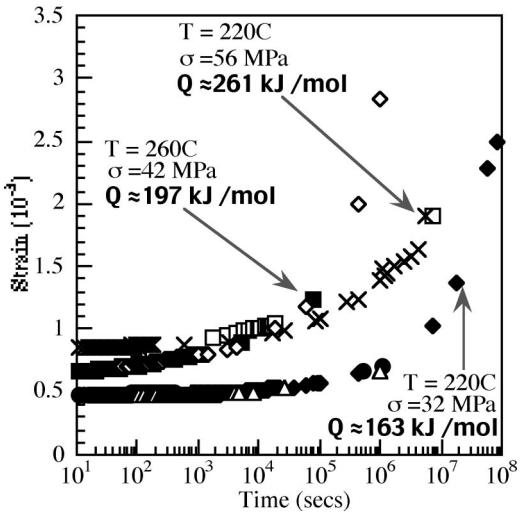

Fig. 4 Master curves obtained for the eutectic alloy from time-temperature superposition to the lowest test temperature. ●: Tested at 31 MPa/220°C, △: Shifted from 31 MPa/260°C, □: Shifted from 31 MPa/280°C, ■: Tested at 42MPa/260°C, ◇: Shifted from 42 MPa/280°C, *X*: Tested at 56 MPa/220°C, □: Shifted from 56 MPa/260°C.

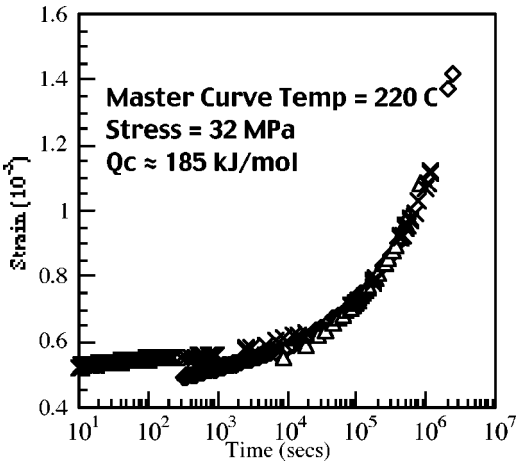

Fig. 5 Master curve obtained for the Al-17Si alloy from time-temperature superposition to the lowest test temperature (220 C). *X*: Original results from 31 MPa-220°C ◇: Shifted from 31 MPa-280C △: Shifted from 31 MPa-260C.

re-expansion can be significant. Blisters were more noticeable near the end of the specimen corresponding to the overflow gate during manufacture, where porosity tends to be highest.

Figures 3(*a*–*d*) show creep curves of strain as a function of time for all three alloys. Fig. 3(*a*) is a log-log strain-time plot of the results for the eutectic alloy for at a temperature of 220°C and a range of stress, while Fig. 3(*b*) shows the results for the eutectic alloy at temperatures of 260°C and 280°C. Fig. 3(*c*) is a comparison of the eutectic and Al-17Si alloy at a constant stress of 32 MPa and varying temperature, while Fig. 3(*d*) shows curves for the eutectic and B390 at a constant stress of 32 MPa and varying temperature.

To compare creep curves, curve fits of the form shown in Eq. (2) were used. In almost all cases the values for the creep exponent, n, were found to be on the order of 0.32 with A as a free parameter. Since $n<1$, the material is still in the primary creep regime. A value of $n=1$ would indicate a steady state (secondary creep) regime and allow the use of Eq. (1) for modeling purposes. The largest values of strain obtained to fracture were on the order of 0.3 percent strain. This indicates: (i) the material never reaches steady state creep; (ii) there is a single rate controlling process which also dictates the fracture mode. From Fig. 3, it can also be qualitatively seen that the eutectic alloy displays a slower creep rate and longer times to failure compared to both of the hypereutectic alloys over the entire testing window. The Al-17Si alloy has a higher strains to failure than the B390. Comparison between the two hypereutectic alloys is complicated by the nature of the manufacturing defects previously discussed.

Master curves were generated by shifting curves horizontally on the log time scale to the lowest test temperature for a given stress (Figs. 4 and 5). This procedure is used for both polymers [17] and for metals [15]. The shifts were used to determine Q_c by application of Eq. (5). Considering first the eutectic Al-Si (Fig. 4), the activation energies acquired were 163, 197 and 261 kJ/mol for stresses of 32, 42, and 56 MPa respectively. It should be noted that the activation energies almost scale linearly with stress, where Q_c (56 MPa) is almost exactly 1.33 times greater than Q_c (42 MPa) and Q_c (42 MPa) is slightly greater than 1.3 times Q_c (32 MPa).

Master curves were also obtained for the Al-17Si alloy (Fig. 5) resulting in Q_c (32 MPa) on the order of 185 kJ/mol. This result is surprising as it would be expected that the activation energy for the material that performs worst be the lowest. At this time the data are too sparse for the B390 to acquire a reliable value for Q_c, but further studies are being conducted.

The master curve approach (time-temperature superposition) is strictly valid for linear systems or for a subset of nonlinear systems in which the shift is independent of stress. Since the shift

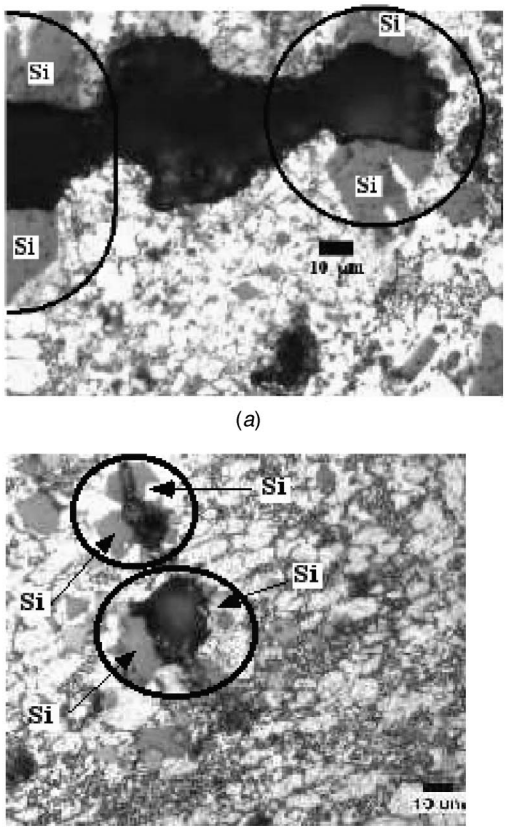

Fig. 6 (*a*) Example of a cracked silicon particle in the Al-17Si alloy: The gray areas are primary silicon phases; and (*b*) example of a cracked silicon particle in the eutectic Al-Si alloy: The gray areas are primary silicon phases.

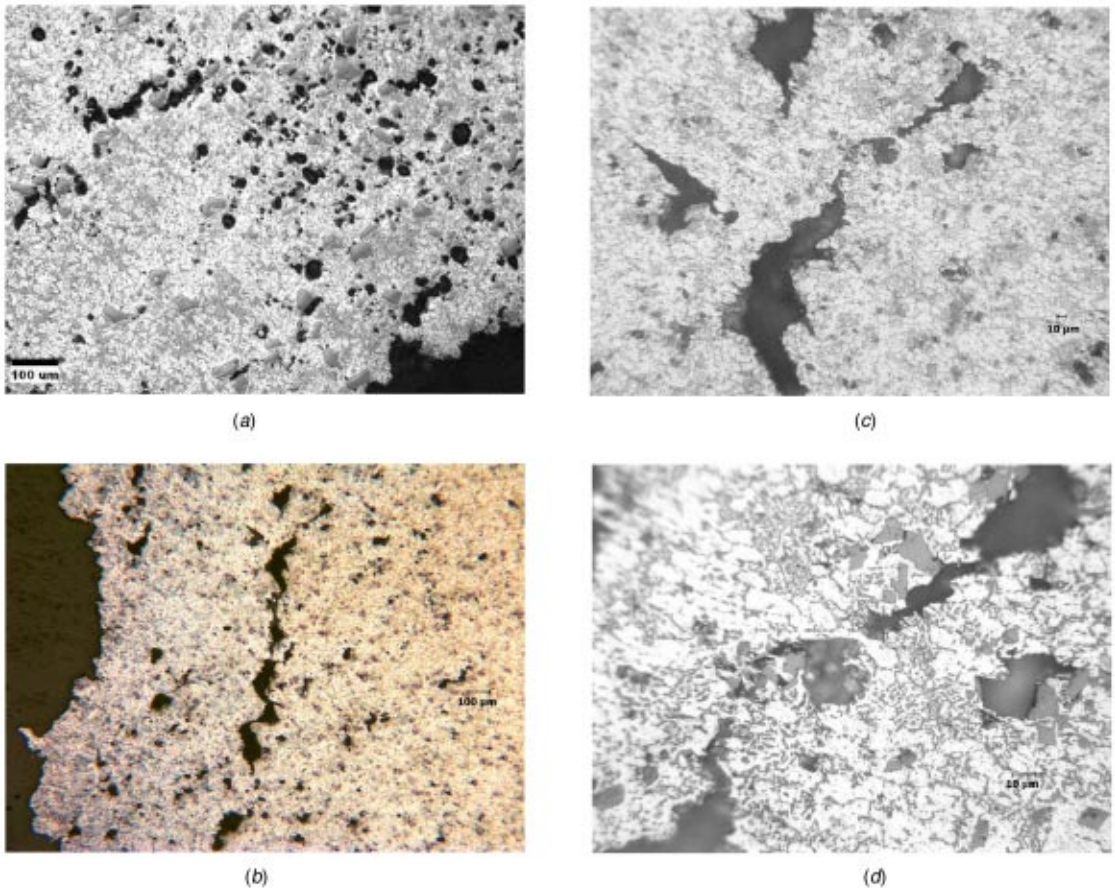

Fig. 7 (*a*) Cavity coalescence along lines perpendicular to stress direction in a fractured Al-17Si creep specimen; (*b*) Sub-fracture crack due to the coalescence of cavities in the eutectic alloy; (*c*) Enlarged view of the crack tip showing crack growth into new cavities; and (*d*) Further enlargement of the crack tip showing cracked silicon particles and void growth on the Si-Al interfaces aiding crack propagation.

factors in the present study depend on stress, the activation energies obtained from them are not directly representative of a fundamental linear process on the atomic scale. Nevertheless, the master curve can be used empirically to extrapolate results to time scales too long to be practical in experiments. Caution is needed since, as seen in Fig. 5, the overlap of shifted curves is not exact. Nonlinear superposition methods are required to accurately model these materials in a more general sense since the time dependent response depends on stress and temperature [9].

The size of the primary silicon particles can be correlated to the creep performance. Analysis of micrographs of crept specimens revealed that large silicon particles were highly susceptible to brittle creep fracture. Figures 6(*a–b*) show examples of cracked particles in crept specimens. From the data in Fig. 3 and the qualitative silicon sizes as seen in Figs. 1 and 2, it can be said that a larger silicon particle size, especially in the presence of other defects, will increasingly degrade creep performance.

Silicon is added to aluminum to increase stiffness, improve wear resistance and to maintain melt fluidity during casting. However, as stated by Kim et al. [3] the formability of these alloys is limited by rupture of the silicon particles, as was also found in this study. Additionally, they were able to achieve superplasticity in a hyper-eutectic alloy of similar composition (Al-25Si-3.7Cu-1Mg-0.42Fe) by greatly refining the silicon grain size through forging. This suggests that the creep resistance, or at least strains to failure, of the alloys examined in this study could be increased through refinement of the primary silicon particles, although methods other than post-casting mechanical deformation would have to be used. This is consistent with the qualitative observation of degraded creep performance with increased silicon particle size seen in this study.

Fracture of all specimens was brittle and intra-granular with no evidence of necking. Cavity coalescence (Fig. 7*a–d*) and crack growth were deduced as the failure mechanism. Low fracture strains are attributed to the fact that cavities are both pre-existing and grown during creep, which makes prediction of time to failure using creep damage parameters, such as the Larsson-Miller and Sherby-Dorn parameters [7], difficult as manufacturing defects vary for each casting.

4 Conclusions

Constant load creep tests were studied for one eutectic and two hyper-eutectic Al-Si alloys. Activation energies were calculated using time-temperature superposition with an assumed a temperature independent Q_c. However, it was shown that, in fact, the materials studied do not obey linear time temperature superposition as the effective activation energy, Q_c, of the eutectic alloy scaled, almost linearly, with stress. Thus, these activation energies are not directly representative of a fundamental atomic scale linear process. They are reported to provide a limited predictive capacity for industrial designers. It was found that the eutectic alloy had larger strains to failure and longer rupture times than the two hyper-eutectic alloys. Most of the creep strain observed was due to irreversible local damage accumulation, though an unreported macroscopic recovery of a small component of strain upon un-

loading was observed in some tests. Brittle fracture of the primary silicon particles was found to be the major factor contributing to poor creep performance, coupled with the presence of other manufacturing defects.

It was observed from the acquired results that all specimens failed in the primary creep regime. Therefore, modeling of the creep-strain histories was done using the modified Andrade Law, as shown Eq. (2), by letting n be a free parameter. However, through curve fitting, it was found that n was on the order of 0.32 for all cases. Based on these results, it can be assumed that these alloys display the same behavior normally described by Andrade's Law with a exponent equal to 1/3. However, use of nonlinear superposition methods is required to full characterize these materials over a range of stress and temperature

References

[1] Ishikawa, K., Maehara, M., and Kobayashi, Y., 2002, ''Mechanical Modeling and Microstructural Observation of Pure Aluminum Crept Under Constant Stress,'' Mater. Sci. Eng., A, **A322**, pp. 153–158.

[2] Timothy, G. J., and Farghalli, M. A., 2002, ''Evidence for Dynamic Recrystallization During Harper-Dorn Creep,'' Mater. Sci. Eng., A, **A322**, pp. 148–152.

[3] Kim, W., Yeon, J. H., and Lee, J. C., 2000, ''Superplastic Deformation of Spray-Deposited Hyper-Eutectic Al-25Si Alloy,'' J. Alloys Compd., **308**, pp. 237–243.

[4] Bae, D. H., and Ghosh, A. K., 2002, ''Cavity Formation and Early Growth in a Superplastic Al-Mg Alloy,'' Acta Mater., **50**, pp. 511–523.

[5] Spigarelli, S., Cabibbo, M., Evangelista, E., and Langdon, T. G., 2002, ''Creep Properties of an Al-2024 Composite Reinforced With SiC Particulates,'' Mater. Sci. Eng., A, **A328**, pp. 39–47.

[6] Ma, Z. Y., and Tjong, S. C., 2000, ''High-Temperature Creep Behavior of SiC Particulate Reinforced Al-Fe-V-Si Alloy Composite,'' Mater. Sci. Eng., A, **A278**, pp. 5–15.

[7] Nabarro, F. R. N., and de Villiers, H. L., 1995, *The Physics of Creep*, Taylor and Francis, London.

[8] Kalpakjian, S., 1997, *Manufacturing Processes for Engineering Materials*, Addison Wesley Longman.

[9] Lakes, R. S., 1998, *Viscoelastic Solids*, CRC Press.

[10] Raj, S. V., 2002, ''Power-Law and Exponential Creep in Class M Materials: Discrepancies in Experimental Observations and Implications for Creep Modeling,'' Mater. Sci. Eng., A, **A322**, pp. 132–147.

[11] Sherby, O. D., and Taleff, E. M., 2002, ''Influence of Grain Size, Solute Atoms and Second-Phase Particles on Creep Behavior of Polycrystalline Solids,'' Mater. Sci. Eng., A, **A322**, pp. 89–99.

[12] Langdon, T. G., 2000, ''Identifying Creep Mechanisms at Low Stresses,'' Mater. Sci. Eng., A, **A283**, pp. 266–273.

[13] Cottrell, A. H., 1996, ''Andrade Creep,'' Philos. Mag. Lett., **73**(1), pp. 35–37.

[14] Nabarro, F. R. N., 1997, ''Thermal Activation and Andrade Creep,'' Philos. Mag. Lett., **75**(4), pp. 227–233.

[15] Nowick, A. S., and Berry, B. S., 1972, *Anelastic Relaxation in Crystalline Solids*, Academic, NY.

[16] Ragab, A. R., 2002, ''Creep Rupture Due to Material Damage by Cavitation,'' ASME J. Eng. Mater. Technol., **124**, pp. 199–205.

[17] Ferry, J. D., 1970, *Viscoelastic Properties of Polymers*, 2nd ed., J. Wiley, NY.